AEÜ, Vol. 48
(1994), No. 6

A Wideband Impulsive Noise Survey in the German Telephone Network: Statistical Description and Modeling

Werner Henkel and Thomas Keßler

Dedicated to Hans-Werner Wellhausen on the occasion of his 60th birthday

A Wideband Impulsive Noise Survey in the German Telephone Network: Statistical Description and Modeling

Results of a measurement campaign carried out in the network of Deutsche Bundespost Telekom are presented. These measurements were conducted at seven locations within Germany. They consisted of the recording of impulses and inter-arrival times and the determination of voltage histograms. The data were used to derive analytical models for the statistics of impulsive noise including the probability density functions of the voltages, the impulse lengths, and the inter-arrival times and the mean power-density spectrum together with phase properties. Proposals for the realization of the statistics in the form of dedicated noise generators inside computer simulation programs are made. Furthermore, a 'representative' impulse, corresponding to the spectral properties, is derived.

Breitbandige Messung von Impulsstörungen im deutschen Telefonnetz: Statistische Beschreibung und Modellierung

Es werden die Ergebnisse einer Meßkampagne im Netz der Deutschen Bundespost Telekom dargestellt. Die Messungen wurden in sieben verschiedenen Ortsnetzen durchgeführt und bestanden aus der Aufzeichnung von Impulsen, Impulsabständen und der Bestimmung von Spannungshistogrammen. Aus den Daten wurden analytische Modelle der statistischen Eigenschaften von Impulsstörungen gewonnen. Diese beinhalten die Verteilungsdichten der Spannungen, der Impulsdauern und der Impulsabstände. Ferner wurden spektrale Eigenschaften in der Form der mittleren Leistungsdichte zusammen mit einer Beziehung für die Phase einbezogen. Darauf aufbauend wird ein Vorschlag zur Realisierung der Statistiken mit speziellen Zufallszahlengeneratoren zur Anwendung bei der Rechnersimulation erarbeitet. Zusätzlich wird ein 'repräsentativer' Impuls, der die spektralen Eigenschaften wiedergibt, ermittelt.

1. Introduction

Non-stationary impulsive noise is a long noticed disturbance in subscriber-line transmission. It is due to internal or external switching or impulse events. Externally induced impulses may originate from high-voltage devices, railways, fluorescent tubes, lightning, etc., whereas the internal ones are caused by the signaling in form of dialing pulses, busy signals, ringing, etc.. These signals are transmitted in two different ways, symmetrically or non-symmetrically relative to ground. Most critical is the non-symmetric transmission, because the NEXT (near-end crosstalk) frequency response is worse compared to the symmetrical case.

Although mechanical switches are increasingly replaced by digital ones, and impulsive noise caused by the switches itself will become more seldom, for the time being, a certain percentage of mechanical switches is still in duty. Telekom intends to replace all mechanical switches until the year 2000. Nevertheless, high-speed digital transmission on subscriber lines is on the way. Hence, newly proposed transmission methods have still to tolerate impulsive noise.

Received May 21, 1994.

Dr.-Ing. W. Henkel, Dipl.-Ing. T. Keßler, Deutsche Bundespost Telekom, Research Center, P.O. Box 10 00 03, D-64276 Darmstadt, Germany, E-mail: henkel@fz.telekom.de or kessler@fz.telekom.de.

Since the early sixties [1–11], impulsive noise studies have repeatedly been the subject of investigations. These were mostly reasoned by the upcoming of digital transmission over telephone lines, at the beginning by means of low bit rate modems. Increasing transmission rate required more and more exact analysis of impulsive noise. The recent introduction of high-speed transmission over subscriber lines with HDSL (high bit rate digital subscriber line) or ADSL (asymmetrical digital subscriber line) initiated new impulsive noise studies. Especially in the case of ADSL, impulsive noise is the major disturbance, because for pure ADSL transmission inside a cable, near-end crosstalk from other ADSL lines is completely avoided due to the duplex transmission in different frequency bands.

The existing examinations were either based on sample measurements at a few locations, mostly narrow band, or on theoretical considerations on the possible impulse-generation mechanism. However, this theoretical work did not deliver a closed analytic description of impulsive noise. Neither did the empirical measurements lead to a closed statistical model. Nevertheless, a few important papers and their results should be mentioned shortly.

A campaign by British Telecom (see, Cook [10]) was carried out with an equipment based on a filter bank for spectral decomposition. It led to the definition of a so-called 'symbolic pulse'. As the shapes of impulses can differ significantly even on one line, such 'representative impulses' should always be handled with caution.

Especially, the impulse proposed in [10] has not a shape similar to real measured impulses. It was defined as

$$h(t) = \begin{cases} V_p|t|^{-3/4}, & t > 0 \\ 0, & t = 0 \\ -V_p|t|^{-3/4}, & t < 0 \end{cases} \quad (1)$$

Unfortunately, it also has a pole at time zero and infinite energy. To be sincere, we should say that besides the statistical model described herein, we searched for possibilities to derive representative impulses, too. However, these impulses were chosen to represent at least both the mean power-density spectrum *and* the impulse phase, but one impulse can, of course, not represent the statistical properties. Its use should therefore be restricted to tests of transmission devices.

Another survey by Bellcore (Valenti and Kerpez [11]) was similar to the one described herein, but the number of sampled impulses and the number of samples taken for histograms were too small to be able to derive statistical properties. Additionally, there were some shortcomings in the analysis of the data.

As more theoretical works, a paper by Berger and Mandelbrot [2] and one by Fano [4] should be cited, where the latter is partly based on the first. Fano's paper yields a complementary distribution of the inter-arrival times as a product of a Pareto-type distribution and an exponential density. Additionally, he averaged over the mean frequency of impulses.

Fano's proposal will be used as one of two possible approaches to approximate the measured inter-arrival time distributions. Especially, for measurements with strongly varying mean impulse frequency, which can be the case, when measurements last very long, including days and nights, the averaging will prove to be useful.

In the following section, our measurements are described in some detail. Thereafter, in Sections 3 to 5, modeling functions for the densities of the voltages, the inter-arrival times, and the impulse lengths, respectively, are proposed. In Section 6, spectral properties in the form of the power-density spectrum are discussed, whereas the next section is devoted to the phase properties of the impulses. Combining phase and amplitude informations, a 'representative' impulse will be derived. A possible simulation scheme is presented in Section 8, including proposals for software generators for the given density functions and methods to incorporate spectral properties. Finally, some concluding remarks will give a short overview of the results.

2. Measurement Description

The survey was intended to cover several locations inside Germany, including at least one in the former GDR (East Germany), where the old switching systems (step-by-step selectors) and cables are notorious for strong impulsive noise. Seven locations were chosen for the campaign (see, Table 1).

The impulsive noise was measured mostly at the end of pairs within inter-office trunks at the main distribution frame inside several local switching offices. There, impulsive noise events occur very often, because signaling c-lines are included in the same cable or even in the same star quad of the cable. This made it possible to come to a sufficient statistical analysis within an acceptable period of time and, furthermore, we could easily install our measurement equipment inside the local offices.

Additionally, one measurement was carried out at a real subscriber line (Darmstadt). The comparison showed that the statistics of impulsive noise on trunks are similar to the ones on the subscriber line.

At every location, the lines were chosen to be out of service and to carry relatively strong impulsive noise (except the measured subscriber line). At one end of the line, a 124-Ω termination was provided, at the other end, the measurement equipment was installed.

The equipment consists of an amplifier and trigger unit, an analog anti-aliasing filter, and a processing storage oscilloscope PSO, i.e., a transient recorder with a built-in PC.

The measured voltage at the end of a pair is symmetrically amplified (27 dB) and low-pass filtered (cut-off frequency at 4.25 MHz). The trigger unit yields a trigger pulse (duration 4.7 μs) when the amplified voltage exceeds an adjustable positive or negative threshold. The filtered signal is sampled at a clock rate of 10.24 MHz ($\hat{=}$ 10 · 1.024 MBaud) and A/D converted (12 bit resolution). The measured data can be stored on a 540-MByte hard disk.

For the model of the impulsive noise, a large number of recorded impulse events and inter-arrival times are necessary. Additionally, histograms of the voltages and peak voltages (sometimes also of the lengths) of the impulse events are determined on-line in order to save storage space.

In the sequel, four different measurements are described, which run fully automatically due to self-developed control routines.

2.1 Recording of Impulses

First, the amplified voltage is adjusted to be DC free and an appropriate trigger threshold has to be chosen. The threshold should be at least twice as high as the inspected level of the Gaussian-like[1] background noise in order to capture more high-amplitude impulses than low ones and to be sure not to record only background noise. This Gaussian level was assumed to be the maximum of the background noise displayed on the PSO.

When a trigger pulse occurs, 4096 successive samples are recorded, 200 of them before the trigger event and 3896 after it. These 4096 samples form a so-called block, corresponding to a period of 400 μs which contains at least one impulse event. After recording 256 blocks triggered successively, they are stored in a file on the hard disk. At every location, 200 files with 256 blocks each were produced which contain the total of about 50,000 impulse events.

[1] Gaussian-like, because actually, the background noise may rather be modeled by a clipped Gaussian density

2.2 Histograms of Voltages

In order to determine histograms of voltages, i.e., the $2^{12} = 4096$ A/D-converter values, the PSO is not triggered by the impulses but runs freely with the sampling clock of 10.24 MHz internally divided by 100 (9.8 μs spacing). This reduced sampling rate ensures, not taking too many samples of one impulse.

After recording 2^{21} samples, their frequency distribution is calculated. Then, by means of this current distribution, the one of previous measured values is updated and the samples are deleted. The control routine alternates between the two modes of recording new samples and of calculating the distribution. During the second mode, no samples are recorded. The histogram measurement at each location took 3 to 7 days and produced up to 10^{10} samples.

Histograms are also derived from recorded impulses, where every sample is evaluated (not every 100th).

2.3 Measurements of Inter-Arrival Times

In the measurement of the inter-arrival times, the same trigger threshold as for the recording of the impulses is chosen. Now, the outputs of a 32-bit counter are recorded at the trigger events instead of the signal samples. The counter is incorporated into the PSO and is clocked at 10.00 MHz.

Inter-arrival times greater than 7.2 min are interpreted wrong, because the counter is limited to a width of 32 bit. Since the relative frequency of inter-arrival times in the range between 6.6 and 7.2 min never exceeded 10^{-6}, this error is negligible.

The inter-arrival times could not be recorded all the time without any interruption, because during the hard-disk access, the counter equipment is out of operation. This does not affect the statistical analysis and is, of course, also true during the voltage-histogram updates (Sections 2.2 and 2.4). The measurement of the inter-arrival times could not be performed simultaneously with the recording of impulses. 16 million counter outputs per location were recorded during 1 or 2 weeks.

2.4 Histograms of Peak Voltages

Histograms of peak voltages were measured on-line at three locations. The control routine alternates between the recording of 4×256 blocks with impulse events and the calculating of the frequency distribution. From each block of 400 μs, the minimum and maximum sample is determined and counted. If the measured signal has been adjusted to be DC free, every block delivers a positive and a negative peak value.

3. Probability Density Function (PDF) of Voltages of Impulsive Noise Samples

As already mentioned, two types of histograms $h(u)$ were used to determine an approximation of this density. One is the 'free-running' histogram, where every 100th sample is taken, regardless of the actual amplitude; the other is derived from recorded impulses, where each sample is evaluated. Both types differ in the percentage of time where only Gaussian background noise (e.g., crosstalk noise) is present. Thus, especially most of the samples of free-running histograms do not belong to the impulses itself, but to background noise. This results in central parts (parabola, due to the logarithm of a Gaussian density) of the histograms with relatively high frequencies. Figure 1a shows such a histogram obtained in the eastern part of Berlin (former GDR), which illustrates the addition of an impulsive noise density and a Gaussian background-noise component. Some of the measurements had virtually no background-noise component, which results in a density with a spike at zero.

In histograms from recorded impulses the spike is smoothed by the additional background noise, but they have not such a dominant Gaussian component in the center. A histogram from recorded impulses is given in Fig. 1b. However, this resulted from a measurement in Mainz (Mayence) that was essentially background-noise free. The local maxima at the edges of the histogram exist only in some of the histograms derived from sampled impulses and result from taking every sample, thereby enabling one single impulse to have a great influence on low-frequency parts of the histogram.

A quite good approximation of the pure impulsive noise density of the voltage u was achieved by[2]

$$f_i(u) = \frac{e^{-|u/u_0|^{1/5}}}{10\Gamma(5)u_0} = \frac{e^{-|u/u_0|^{1/5}}}{240u_0}, \qquad (2)$$

a double exponential with a power of 1/5 in the exponent and with the parameter $u_0 > 0$ V. If we include background noise which is the only disturbance *between* impulses, we obtain the sum

$$f_{tot}(u) = N f_n(u) + (1 - N) f_i(u) * f_n(u), \qquad (3)$$

where

$$f_n(u) = \frac{1}{\sigma\sqrt{2\pi}} e^{-u^2/(2\sigma^2)}$$

is the density of the Gaussian noise with the standard deviation σ and $N \in [0, 1]$ is its relative portion. *During* an impulse, background noise is there, too. Thus, assuming statistical independence between both processes and stationarity within the duration of the impulse, the addition of the two disturbances results in the convolution of their densities.

Fig. 1b shows the approximation with the pure impulsive noise density, eq. (2), whereas in Fig. 1a an approximation according to eq. (3) has been performed. The component functions (Gaussian background-noise density, impulsive noise density, and convolution result) are given in Fig. 2.

Approximation results from eight data sets at different locations are presented in Table 1. The utilized

[2] $\Gamma(x)$: Gamma function

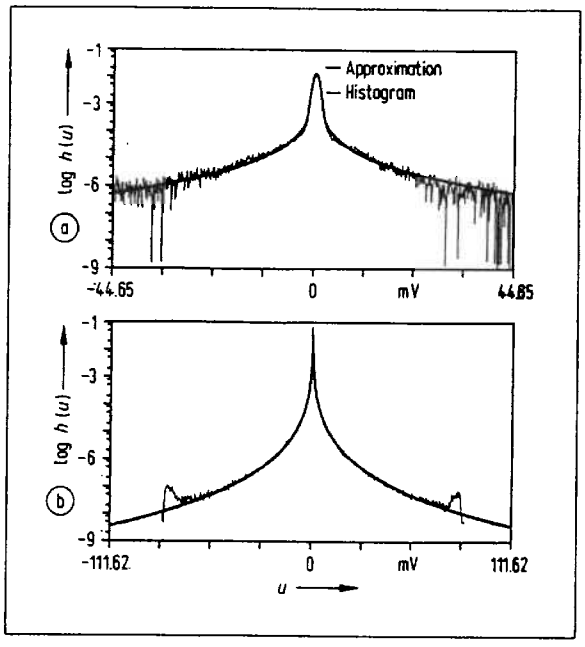

Fig. 1. Approximation of an impulsive noise voltage density with background noise (a) in Berlin and (b) with low background noise in Mainz.

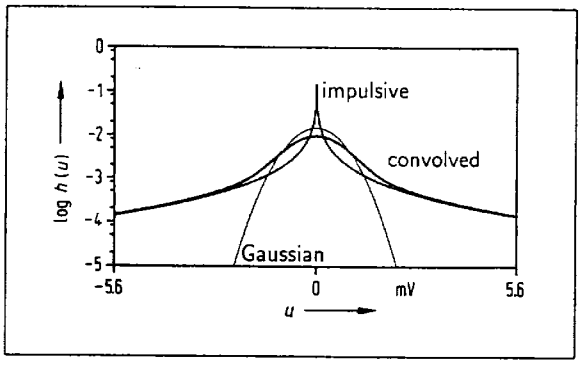

Fig. 2. Component functions of the approximation in Fig. 1a.

interactive graphical tool comprises routines for nonlinear and linear approximation. The histogram was separated into two parts dominated by Gaussian background noise and impulsive noise, respectively. The special shape of the two densities has the advantage that the convolution according to (3) does only lead to some modifications of the shape in the areas where the Gaussian component in the center goes over to the impulsive component outside. Note that the impulsive density has a spike in the middle which has a Dirac-like effect when convolved with the Gaussian density. Thus, the shape of the Gaussian density is nearly left unchanged. Furthermore, the Gaussian density is rather narrow relative to the slope of the impulse density outside the center area. Hence, this slope is also not modified significantly by the convolution. This allows the applied separate approximation.

Besides the densities of voltages (Section 2.2), histograms of peak voltages (Section 2.4) might be of

Table 1. Approximation parameters for the voltage-frequency distributions.

Location	N	σ (mV)	u_o (nV)
Darmstadt	0.991	0.19	0.7
Ober-Ramstadt	0.999	0.54	20.9
Frankfurt (72)	0.947	0.55	46.6
Frankfurt (23)	0.972	0.48	5.9
Biebergemünd	0.803	1.17	63.9
Kassel	0.946	–	1.4
Berlin	0.706	0.60	123.1
Mainz	0.996	–	18.2

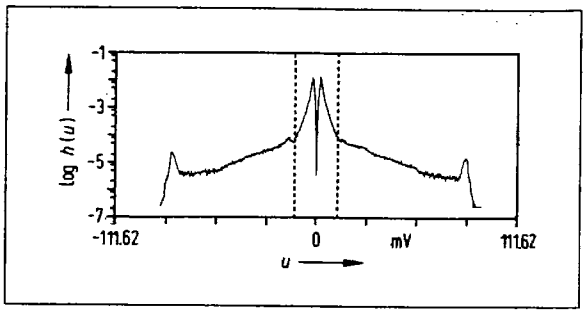

Fig. 3. Frequency distribution of the impulse peak voltages (Mainz).

interest, too, although they are not needed for our modeling. One such histogram is depicted in Fig. 3. Notable is the possibility to distinguish between two different parts (partitioned by two symmetrical bends at about ± 12 mV; see, dotted lines) that might be due to different physical phenomena. These two different sections of such histograms have also been realized in former surveys [9].

4. PDF of Inter-Arrival Times

The inter-arrival times were calculated as the difference of the recorded counter outputs (cf., Section 2.3) at trigger instants. In order to determine the frequency distribution, $2^{32} \approx 10^9$ possible inter-arrival times were divided into exponentially spaced classes. Thus, densities $f_{\log_{10}(t/100\text{ns})}(\log_{10}(t/100\text{ns}))$ are considered. The densities of the inter-arrival times will be derived from the densities of logarithmic times by applying the well-known transformation rule. A substitution of a variable x inside a density function $f(x)$ by another variable $x(\xi)$, changes the density according to

$$f(\xi) = f(x(\xi))\,|\mathrm{d}x(\xi)/\mathrm{d}\xi|\,. \qquad (4)$$

Two exemplary frequency distributions $h(\log_{10}(t/100\text{ns}))$ are shown in Fig. 4 in logarithmic representation[3], where separate curves for day and

[3] The distributions start from 4.7 μs due to the duration of the chosen trigger signal.

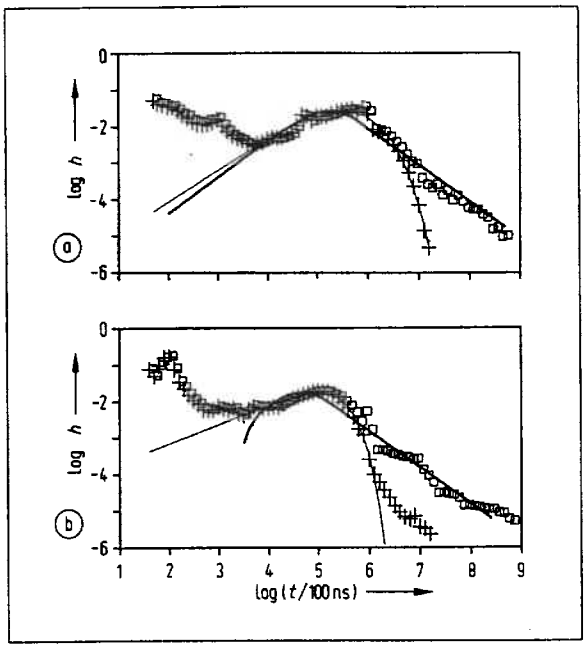

Fig. 4. Approximation of the density of the logarithm of the inter-arrival times: (a) Kassel, (b) Frankfurt. (□) Measurement, days and nights; (+) Daytime measurement; (−) Generalized exponential density, eq. (9); (—) Average over exponential/Pareto density, Fano [4].

nighttime and only daytime are drawn. The frequency distributions show a maximum at $t \approx 30$ ms, due to the transformation. Short inter-arrival times up to a certain time span occurred more often than a Poisson process would produce. Since they can be seen as gaps within impulses, they were not considered. Hence, approximations were performed starting from about 100 μs.

Also for higher inter-arrival times, the measured densities could not be modeled by the usual Poisson process, because the mean impulse frequency λ, which is proportional to the calling rate, varies during the measurement. A solution is to average the exponential density over a range of the mean impulse frequency $0 \le \lambda \le \lambda_0$ assuming a uniform distribution over that range as proposed in [4] by Fano. This results in the complementary distribution and density

$$1 - F(t) = \frac{1}{\lambda_0}\int_0^{\lambda_0} \mathrm{e}^{-\lambda t}\mathrm{d}\lambda = \frac{1-\mathrm{e}^{-\lambda_0 t}}{\lambda_0 t},$$

$$f(t) = \frac{\mathrm{d}F(t)}{\mathrm{d}t} = \frac{1}{\lambda_0 t^2}\left[1-(1+\lambda_0 t)\mathrm{e}^{-\lambda_0 t}\right]. \quad (5)$$

This density seems only to be suited for measurements with strongly varying mean impulse frequencies, which was the case, e.g., in the banking district of Frankfurt. There, almost no impulse occurred during the nights.

Another possibility is to model only for the daytime, because the daytime statistics are more severe and of more interest, anyway. An acceptable approximation was achieved by a generalization of the Poisson law. There, intervals between events are exponentially distributed:

$$f(x) = c_1 \mathrm{e}^{-c_2 x}, \quad x \ge 0, \quad (6)$$

where $c_1 = c_2 = \lambda$ denotes the mean event frequency. We distinguish between c_1 and c_2 to trace their positions in the subsequent derivations.

Applying (4) with $x = 10^\xi$, we obtain

$$f(\xi) = c_1 \mathrm{e}^{-c_2 10^\xi} \ln(10) \cdot 10^\xi. \quad (7)$$

In logarithmic representation this can be written as

$$\log_{10}(f(\xi)) = \log_{10}(c_1 \ln(10)) + \xi - \frac{c_2}{\ln(10)} 10^\xi. \quad (8)$$

We generalize as follows:

1) Constant $\log_{10}(c_1 \ln(10)) \longrightarrow a_1$
2) Linear term $\xi \longrightarrow a_4 \xi$
3) Basis 10 $\longrightarrow a_2$
4) $c_2 \longrightarrow a_4$ and exponent $\xi \longrightarrow (\xi - a_3)$

The position of the maximum is now determined by a_3 instead of c_2. a_4 specifies the slope of the curve at its beginning and a_2 defines the radius of the curvature at the maximum. a_1 is a normalization constant.

Thus, we obtain the generalized exponential density

$$\log_{10}(f_d(\xi)) = a_1 + a_4\xi - \frac{a_4}{\ln(a_2)} a_2^{(\xi - a_3)}, \quad (9)$$

which again can be rewritten with $\xi = \log_{10}(x)$ as

$$f_d(x) = \frac{10^{a_1}}{\ln(10)} x^{a_4 - 1} 10^{-\frac{a_4}{\ln(a_2)} a_2^{(\log_{10}(x) - a_3)}}, \quad (10)$$

where $x = t/100$ ns. Almost all daytime measurements can be approximated quite well by the inter-arrival time density in (10). Only the right part of the curve in Fig. 4b for $t > 126$ ms cannot be modeled by our approach (strongly varying mean impulse frequencies in the banking district of Frankfurt). However, the approximation will offer a worst case description for this case, too. The approximated parameters a_2, a_3, a_4 are listed in Table 2 for six locations. a_1 has to be determined such that the integral over (10) equals one.

Table 2. Approximation parameters of the inter-arrival times approximation.

Location	a_2	a_3	a_4
Darmstadt	1.68	6.70	0.88
Ober-Ramstadt	6.38	5.43	0.62
Frankfurt (72)	11.17	5.00	0.53
Kassel	5.04	5.62	0.70
Berlin	2.80	5.04	1.91
Mainz	2.22	5.15	1.26

5. PDF of Impulse Lengths

By definition, an impulse event begins, when a certain trigger threshold is exceeded and, beforehand, the voltage has been lower than the 'Gaussian' level for some specified period of time t_D. The impulse event ends at the instant, when it returns and remains for t_D below the 'Gaussian' level. A higher amplitude than the 'Gaussian' level after a time span of more than t_D is considered to belong to another impulse event. $t_D = 100\ \mu s$ has been chosen for all locations. However, a variation of t_D within the range between 10 μs and 1 ms does not affect the distributions significantly (cf., inter-arrival time density). Nevertheless, the length distribution at different locations, determined in such a way, showed the most variations of all statistics.

A typical measured length-frequency distribution $h(t)$ (Fig. 5a) can be approximated by the sum of two log-normal densities

$$f_l(t) = B\frac{1}{\sqrt{2\pi}s_1 t}e^{-[\ln^2(t/t_1)]/(2s_1^2)} + \\ + (1-B)\frac{1}{\sqrt{2\pi}s_2 t}e^{-[\ln^2(t/t_2)]/(2s_2^2)}. \quad (11)$$

t_1, t_2 are the median values and s_1, s_2 are the shape parameters of the log-normal densities.

Smoothed curves of the other locations can be described by eq. (11), too, (Figs. 5b and 5c), even though they have not always the typical shape of Fig. 5a. The approximated parameters for six locations are shown in Table 3. We tried to fix the parameters s_1, s_2, t_1, t_2 in our approximation in order to simplify our model. They were set to

$$\begin{aligned} s_1 &= 7.68 \cdot 10^6, \\ s_2 &= 10.24 \cdot 10^6, \\ t_1 &= 7.2\mu s, \\ t_2 &= 160\mu s. \end{aligned} \quad (12)$$

s_1 and s_2 of eq. (12) are roughly similar to the most entries in Table 3, whereas for t_2 the worst case was chosen. As high median values t_ν are covered by the second log-normal density (t_2), a relatively small value that resulted approximately from the mean of the last two entries was selected for t_1.

The approximation with free parameters is, of course, somewhat better, but it was our intention to develop a model consisting of as few parameters as possible.

6. Properties of the Power-Density Spectrum (PDS)

Assuming an ergodic process, the momentary PDS $L(f)$ can approximately be described by the Fourier transform $S_{T_B}(f)$ over an interval T_B:

$$L(f) \approx \frac{1}{T_B} \mid S_{T_B}(f) \mid^2 . \quad (13)$$

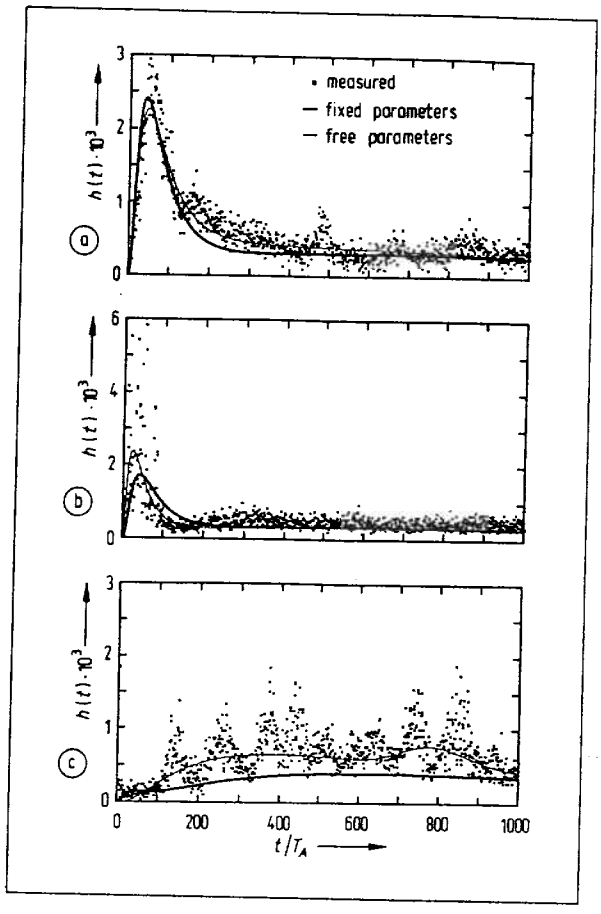

Fig. 5. Approximation of the impulse-length density: (a) Mainz, (b) Darmstadt, (c) Frankfurt. $T_A/10.24\text{MHz} \approx 97.7$ ns.

We use the DFT

$$S_\delta(k) = \sum_{n=0}^{M-1} u_\delta(n) e^{-j2\pi nk/M},\ 0 \le k \le M-1, \quad (14)$$

with $u_\delta(n)$ being the samples of the voltage $u(t = nT_A)$, $T_A = 1/10.24\ \text{MHz} \approx 97.7$ ns, within the interval T_B. The DFT-block size $M = 2048$ corresponds to the chosen interval $T_B = 200\mu s = MT_A$ which is one half of the measured block of 400μs.

At discrete frequencies $f = k\Delta f$, the PDS in eq. (13) can be determined by

$$L_\delta(k) = L(f = k\Delta f) \approx \frac{T_A^2}{T_B} \mid S_\delta(k) \mid^2, \quad (15)$$

where $\Delta f = 1/(T_A M) = 1/T_B = 5$ kHz. The factor T_A^2 is explained, e.g., in [12, p. 27].

Before the FFT transform, the signal was windowed using a convolution of a Blackman-Harris window with a rectangular one[4]. In the frequency domain, the distortion due to the amplifier and low-pass filter was equalized.

[4] The special window function has been chosen because of its negligible effect on the impulse shape and spectrum. However, using this window is not mandatory.

Table 3. Parameters for the approximation of the impulse lengths; $\bar{l}$: mean of the length, 'free': approximation of all parameters, 'fixed': approximation of B with fixed parameters s_ν, t_ν (eq. (12)).

Location	$\bar{l}$ (μs)	B_{fixed}	B_{free}	s_1 ($\times 10^6$)	s_2 ($\times 10^6$)	t_1 (μs)	t_2 (μs)
Darmstadt	87.0	0.178	0.166	8.26	8.96	4.68	128.2
Ober-Ramstadt	101.8	0.051	0.66	14.54	1.71	109.26	107.1
Frankfurt (72)	85.5	0.014	0.94	9.83	1.12	93.10	77. 8
Kassel	81.8	0.118	0.236	6.28	8.14	14.50	108.2
Berlin	95.9	0.063	0.06	7.68	10.44	6.85	158.2
Mainz	93.6	0.250	0.256	7.68	10.63	7.95	125.7

Since the PDS of all impulses varies a lot, the PDS cannot be described generally in an easy way. A multidimensional distribution of the PDS in the form $f_{\mathcal{L}}(\mathcal{L})$, where $\mathcal{L}$ is the vector of the $L_\delta(k)$, $k = 0, \ldots, M-1$, would be necessary. This would be far too complicated. It is more feasible to average over all the recorded impulses. A mean PDS of all measured first block halves ($0 \le t < 200\ \mu$s) at one location is given in Fig. 6a.

Parts of such spectra belonging to Gaussian background noise which is superimposed onto the impulses, were eliminated by subtracting the mean PDS of Gaussian noise from this mean PDS of both impulsive and Gaussian noise. The mean PDS of Gaussian noise is the average of squared absolute FFT values of all measured second block halves ($200\ \mu\text{s} \le t < 400\ \mu$s) which contain no impulses. When subtracting both mean PDS, besides the background noise, discrete spectral lines due to digital baseband transmission in parallel pairs or AM radio, disappear mostly (cf. Figs.6a and 6b).

Figures 6b and 6c show two examples of the mean PDS of pure impulsive noise. Although the mean PDS at different locations are not similar, they can roughly be approximated by one or two straight lines in double logarithmic representation (included in the figures which are linear in f):

$$\overline{L(f)}/\text{dB(pW/kHz)} = \quad (16)$$
$$= \begin{cases} -15\log_{10}(f/\text{Hz}) + \gamma_1, & 5\ \text{kHz} \le f \le f_x \\ -29\log_{10}(f/\text{Hz}) + \gamma_2, & f_x \le f \le 4\ \text{MHz}, \end{cases}$$

where γ_1, γ_2 are constants and f_x denotes the point of intersection. For Mainz, we chose f_x to be 1.64 MHz, $\gamma_1 = 80$, and $\gamma_2 = 167$, whereas for Kassel, only the first line with $\gamma_1 = 70$ may be used.

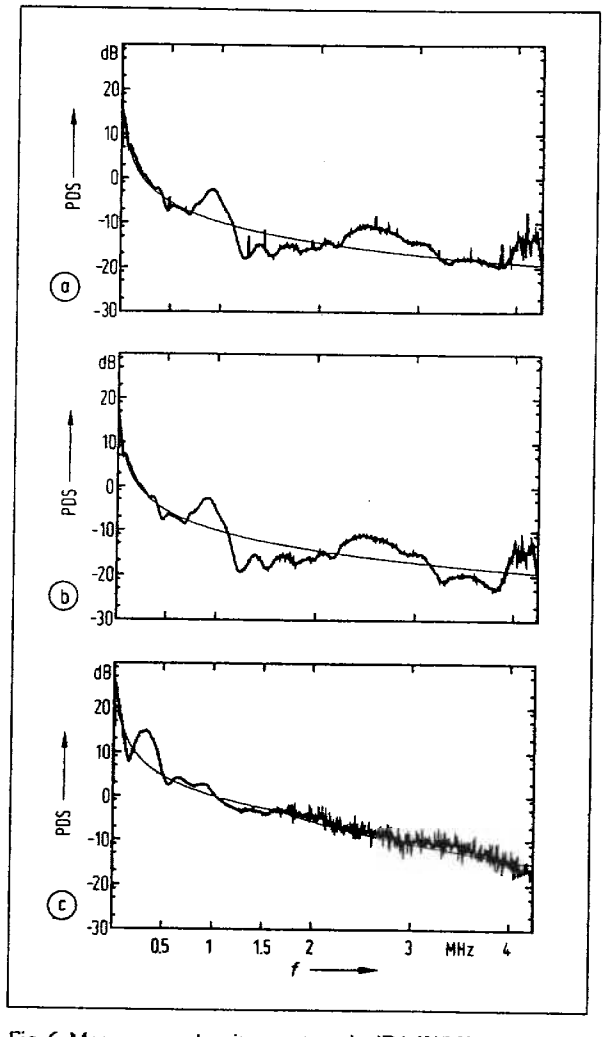

Fig. 6. Mean power-density spectrum in dB(pW/kHz) (a) of both impulsive and background noise recorded in Kassel and of pure impulses recorded in (b) Kassel and (c) Mainz. (—) PDS, (—) Approximation.

7. Phase Properties and 'Representative' Impulse

Up to now, in this paper no effort has been made to model the phase properties of the impulses. Nevertheless, these are important for the impulse shape. Simple solutions would be to set the phase to zero or to use a discrete Hilbert transform [12] based on the square-root of the mean PDS. In the first case, the impulse response is symmetric, while in the latter, the minimum-phase impulse starts with high amplitudes right after time zero. The first approach is used to define the tap coefficients of a filter that will be used for the impulsive noise simulation scheme in Section 8.2, but both alternatives

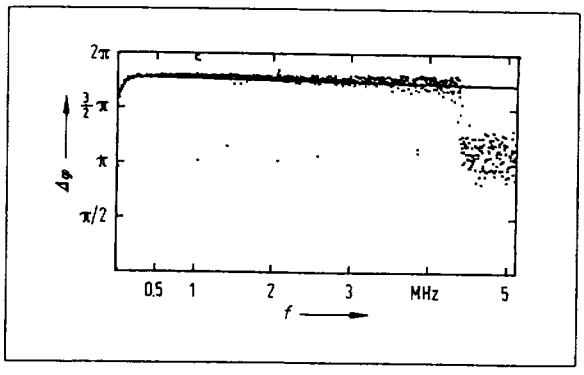

Fig. 7. Approximation of the phase difference (group delay). The dots are the locations of maxima in a histogram of phase differences.

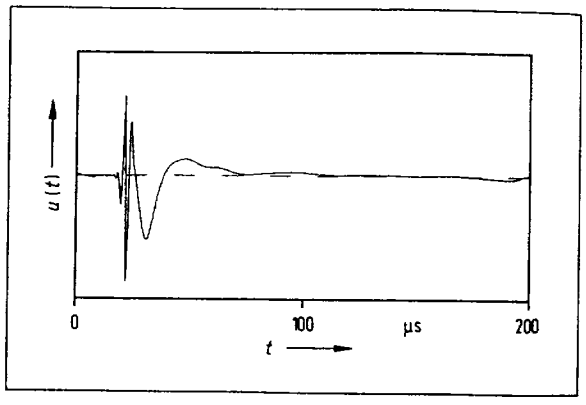

Fig. 8. 'Representative' impulse derived from Fig. 6c and the approximation in Fig. 7.

cannot be used to obtain an impulse shape similar to real measured impulses.

Furthermore, it is not very meaningful to average over the phase of the DFT of recorded impulses, because this would yield zero. However, it showed out that a quantity similar to the group delay $-(1/(2\pi))\mathrm{d}\varphi(f)/\mathrm{d}f$ always follows a simple analytic formula. We observed that the phase difference

$$\Delta\varphi(k\Delta f) = \varphi(k\Delta f) - \varphi((k-1)\Delta f),\ k \geq 1 \quad (17)$$

between neighboring spectral lines of the FFT spectrum can be approximated by

$$\Delta\varphi(k\Delta f) = \phi_0 + \phi_1(1 - \mathrm{e}^{-k/\phi_2}) - \phi_3 k,\quad k \geq 1,\quad \Delta f = 5\,\mathrm{kHz}, \quad (18)$$

with the approximation parameters $\phi_\nu, \nu = 0, \ldots, 3$. A plot of such phase differences together with the approximation according to (18) is given in Fig. 7. To be more precise, the phase differences drawn there are the locations of the maxima in a histogram of phase differences. Actually, the maxima follow the approximation curve only in frequency ranges where the energy spectrum of the impulses have significant values. Otherwise the histogram is dominated by background noise. Especially, above the cut-off frequency of the anti-aliasing filter, the power spectral density is too low to define the corresponding phase difference.

The phase $\varphi(k\Delta f)$ is determined from the approximation of $\Delta\varphi(k\Delta f)$ with the initial condition $\varphi(0) = 0$. From this phase together with the square root of the mean PDS (Fig. 6c), one can compute a 'representative' impulse for a measurement. Figure 8 shows such an impulse that indeed looks like real measured impulses.

Table 4 shows the approximation parameters for different measurements. ϕ_3 always assumed the same value $\phi_3 = 2.1 \cdot 10^{-4}$. The starting values $\Delta\varphi(1 \cdot \Delta f)$ and $\Delta\varphi(2\Delta f)$ are often not too well described by eq. (18) and are then taken from the original data.

Table 4. Parameters of the phase-difference approximation $\Delta\varphi(k\Delta f) = \phi_0 + \phi_1(1 - \mathrm{e}^{-k/\phi_2}) - \phi_3 k$, $\phi_3 = 2.1 \cdot 10^{-4}$.

Location	ϕ_0	ϕ_1	ϕ_2
Darmstadt	3.795	1.355	17.748
Ober-Ramstadt	5.295	0.296	14.764
Frankfurt (72)	5.150	0.376	22.063
Kassel	4.688	0.889	5.685
Berlin	0.000	5.610	1.082
Mainz	4.985	0.624	15.152

8. Impulsive Noise Simulation

This section is devoted to the generation of impulsive noise on the basis of specially developed generators. These generators are described first. Then it is outlined, how spectral properties can be ensured, too. A complete block diagram of the impulsive noise simulator is presented afterwards.

8.1 Generators with the Described Impulsive Noise Statistics

We shall describe possible realizations of pseudo-noise generators for computer simulation that will follow the above-derived densities. The generators utilize well-known principal methods or variations thereof – 'transform method', 'rejection method', 'strip method'.

The *transform method* utilizes the density change when applying a function $\xi(x)$ to a random variable. The density is modified according to (4), which in the sequel is used in an equivalent form with $\mathrm{d}\xi(x)/\mathrm{d}x$ in the denominator.

The **generator for the voltage samples of the impulses** uses the *rejection method* (see [13, pp. 203-206] or [14, pp. 120-121]). Herein, one selects a function $kf_\cap(x)$ according to the condition

$$kf_\cap(x) \geq f_i(x), \quad k \in I\!R. \quad (19)$$

This function should be easily integrable. Additionally, $F_\cap(x) = \int_{-\infty}^{x} f_\cap(\eta)\mathrm{d}\eta$ should also be easily invert-

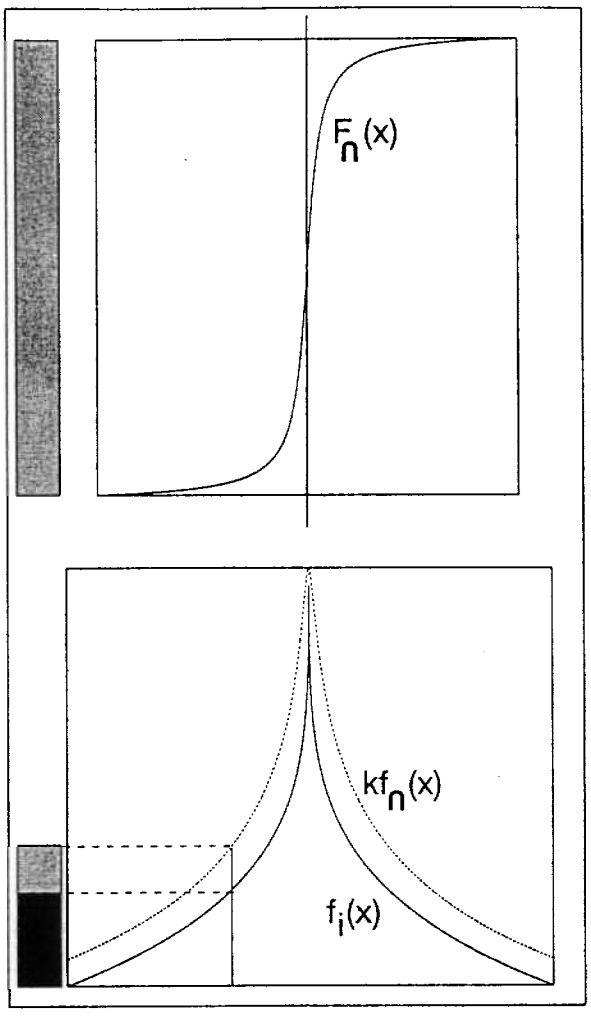

Fig. 9. Rejection method.

ible. The procedure works as follows: x is obtained by applying $x = F_\cap^{-1}(\xi)$ to some uniform (0,1) random number ξ. This can be seen as an application of the transform method, because $f_\cap(x) = f_\cap(F_\cap^{-1}(\xi)) = f_\xi(\xi)/\left|\mathrm{d}F_\cap^{-1}(\xi)/\mathrm{d}\xi\right| = 1 \cdot |\mathrm{d}F_\cap(x)/\mathrm{d}x|$.

Then, $f_\cap(x)$ is multiplied with a constant k, such that the condition (19) is fulfilled. A second uniform $(0, kf_\cap(x))$ generator determines, if x is taken as output or being rejected. Rejection takes place, when the second uniformly distributed random number is greater than $f_i(x)$. The exact value of k does not influence the outcoming distribution, but the speed of the random number generation. The farer $kf_\cap(x)$ is apart from the desired $f_i(x)$, the higher is the percentage of rejected values. Figure 9 describes the procedure.

For the voltage-generator application, we selected $kf_\cap(x)$ and $kF_\cap(x)$ to be

$$\begin{aligned} kf_\cap(x) &= k\frac{c/\pi}{1+c^2x^2}, \\ kF_\cap(x) &= k(\arctan(cx)+\pi/2)/\pi. \end{aligned} \tag{20}$$

The constants k and c are chosen such that condition

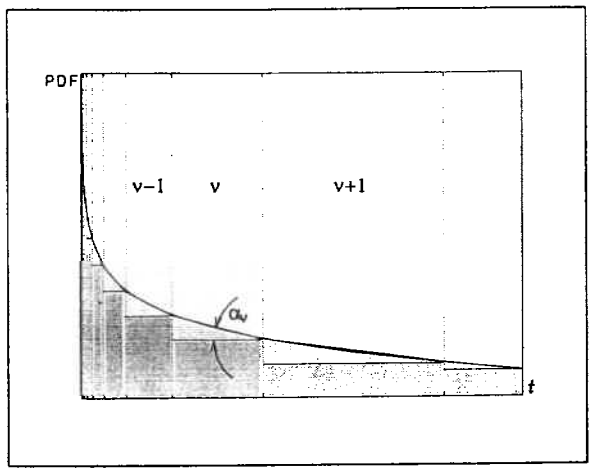

Fig. 10. Modified strip method.

(19) is fulfilled in a certain range, $kf_\cap(0) = f_i(0)$, and $kf_\cap(x)$ is as small as possible.

A solution would be to initialize $f_\cap(\pm u_R) = f_i(\pm u_R)$ at the right and left border of the chosen voltage range $(\pm u_R)$. Then iteratively, c is changed (while $k = \pi/(240u_0c)$) until $\forall x, x \in [-u_R, u_R] : f_\cap(x) \geq f_i(x)$.

The **generator for the inter-arrival times** is based on a modified strip method. In its original form (see, e.g., [15, pp. 359-368], [14, pp. 118-122]) the PDF is divided into N_S strips and the corresponding probabilities $p^{(\nu)}$, $0 \leq \nu \leq N_S - 1$, to obtain a value within a strip, are determined. $p^{(\nu)}$ equals the area of a strip ν. A special random number generator is used to select the strips according to the $p^{(\nu)}$ and afterwards any other procedure is taken to approximate the exact shape of the density within one strip.

For our application, we employ exponentially spaced boundaries (see, Fig. 10) in order to divide the PDF into strips, which again are divided into rectangular regions (probability $p_\square^{(\nu)}$) always below the PDF and triangular ones (probability $p_\triangle^{(\nu)}$), featuring a piecewise linear approximation of the PDF. The strips (regions) are chosen by a random number generator due to Walker [16] (see, below). If a rectangular strip is met, a uniform number generator is used to generate the actual output between the strip boundaries, whereas in the case of a triangular strip, additionally, the transform method with $x(\xi) = \sqrt{\xi}$ is applied.

Let α_ν be the angle of the νth triangular part and $f_g^{(\nu)}(\xi) = 1/2\tan(\alpha_\nu)$ (between the strip boundaries) be the uniform density of a random number generator. With

$$\begin{aligned} x &= \sqrt{\xi}, \\ \mathrm{d}\xi/\mathrm{d}x &= 2x, \end{aligned}$$

and applying (4) we obtain

$$f_\triangle^{(\nu)}(x) = \tan(\alpha_\nu) \cdot x. \tag{21}$$

$f_\Delta^{(\nu)}(x)$ represents the desired (piecewise) linear density.

Maybe, a sketch of Walker's method should be given shortly, too. First, the desired discrete probabilities $(p^{(\nu)})$ are compared with a uniform distribution $(1/N_S)$. The greatest negative (C) and positive differences (D) between $p^{(\nu)}$ and $1/N_S$ are searched. For the position $\nu = \nu_C$ of the greatest negative difference, an 'alias' value ν_D is stored, which is output as an alternative to the original value that corresponds to a certain probability. The greatest negative difference is added to the positive one, thereby reducing this difference. Additionally, a threshold, defined by $1 - CN_S$, is stored. As $1 - CN_S = N(1/N_S - C)$, this threshold corresponds to the difference C. Now, the difference C at position ν_C is reduced to zero. The search for greatest negative (C) and positive differences (D) is repeated until all negative differences have been processed (at most $N_S - 1$ times).

Walker's generator itself is based on some sort of rejection method, in the sense that it accepts values from a uniformly distributed discrete generator, if a second uniformly distributed continuous generator delivers values less than the threshold. If the threshold is exceeded, the 'alias' value is output. For a Fortran routine see [16].

The realization of the **generator for the impulse lengths** is based on a normal (0,1) generator with the density $f_g(x)$ (e.g., polar method by Box, Muller et al.; see [14, pp. 117-118]) together with an exponential function in the transform method:

$$f_g(x) = \frac{1}{\sqrt{2\pi}} e^{-x^2/2},$$
$$t = e^{s_\nu x + \ln(t_\nu)},$$
$$dt/dx = s_\nu t,$$

applying (4):

$$f_l^{(\nu)}(t) = \frac{e^{-[\ln^2(t/t_\nu)]/(2s_\nu^2)}}{\sqrt{2\pi} s_\nu t}, \quad \nu = 1, 2. \tag{22}$$

The addition of two log-normal densities (eq. (11)) is taken into account by choosing the two parameter sets (t_ν, s_ν) randomly with the probabilities B and $1 - B$, respectively.

8.2 Incorporating Spectral Properties

A simple way to ensure spectral properties is to use the noise generators described in the last section followed by an FIR filter. The coefficients of the FIR filter are determined from the square root of the mean PDS of a certain location or of the approximation eq. (16). About 200 coefficients are necessary.

Since the voltage density is changed by the FIR filter, a PDF $f_1(u)$ at the input must be searched that yields the desired PDF $f_i(u)$ at the output. The PDF $f_{out}(u)$ at the output of an FIR filter can be derived as follows:

A multiplication with one coefficient k_ν changes the density according to

$$f_1'(u) = \frac{f_1(u/k_\nu)}{|k_\nu|}. \tag{23}$$

The addition of n, e.g., $n = 200$, random processes results in the convolution of their densities, which would lead to $n - 1$ such convolutions

$$f_{out}(u) = \frac{1}{\prod_{\nu=1}^{n} |k_\nu|} \int_{\eta_{n-1}} \cdots \int_{\eta_2} \int_{\eta_1} f_1\left(\frac{\eta_{n-1}}{k_n}\right) f_1\left(\frac{\eta_{n-2} - \eta_{n-1}}{k_{n-1}}\right) \cdots$$
$$\cdots f_1\left(\frac{\eta_j - \sum_{\mu=j+1}^{\mu=n-1} \eta_\mu}{k_{j+1}}\right) \cdots f_1\left(\frac{u - \sum_{\mu=1}^{\mu=n-1} \eta_\mu}{k_1}\right) \cdot$$
$$\cdot d\eta_1 d\eta_2 \ldots d\eta_{n-1}. \tag{24}$$

This corresponds to a multiplication of the corresponding characteristic functions (the Fourier transforms) $F_1(k_\nu\omega)$

$$F_{out}(\omega) = \prod_{\nu=1}^{\nu=n} F_1(k_\nu\omega). \tag{25}$$

Although (25) is a simplification of (24), it is not possible to construct any analytic expression for f_1, applying this equation. A feasible solution is the superposition of a Dirac onto the PDF of the input process. In our case, the Dirac approximately regenerates the desired PDF. The PDF at the input of the filter is changed according to

$$f_1(u) = \epsilon f_i(u) + (1 - \epsilon)\delta(u) \tag{26}$$

with $\epsilon \in [0.01, 0.1]$.

Note that the convolution of a Dirac with an arbitrary function yields the function itself. Assuming a dominant Dirac component as defined in (26), a convolution of two such functions (transformed with k_ν) results in a sum of four components: a Dirac multiplied with $(1 - \epsilon)^2$, the two functions $f_i(u/k_\nu)/|k_\nu|$ themselves, each multiplied with $\epsilon(1 - \epsilon)$, and a mixed convolution of the two functions $f_i(u/k_\nu)/|k_\nu|$ multiplied with ϵ^2. n such convolutions reduce the pure Dirac component by a factor of $(1 - \epsilon)^n$. The characteristic function corresponding to (26) is given by

$$F_1(\omega) = \epsilon F_i(\omega) + (1 - \epsilon). \tag{27}$$

Inserting (27) into (25), yields

$$F_{out}(\omega) = \tag{28}$$
$$= \sum_{\nu=0}^{n} \left((1 - \epsilon)^{n-\nu} \epsilon^\nu \sum_{(\zeta_1, \ldots, \zeta_\nu) \in C_\nu^n} \prod_{\mu=1}^{\nu} F_i(k_{\zeta_\mu}\omega) \right),$$

where C_ν^n denotes the set of all combinations of ν elements out of a set of n elements. The pure Dirac component corresponds to the constant term for $\nu = 0$.

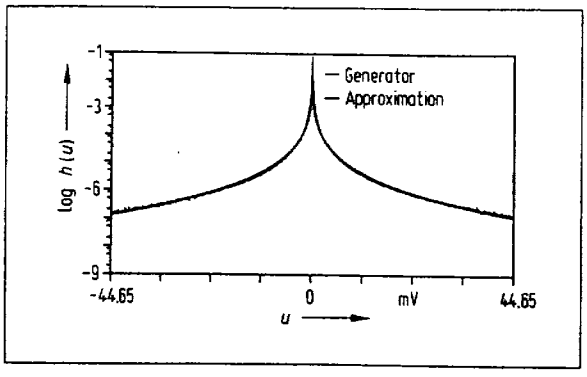

Fig. 11. Frequency distribution at the output of a filter with a response of the square root of the power-density spectrum.

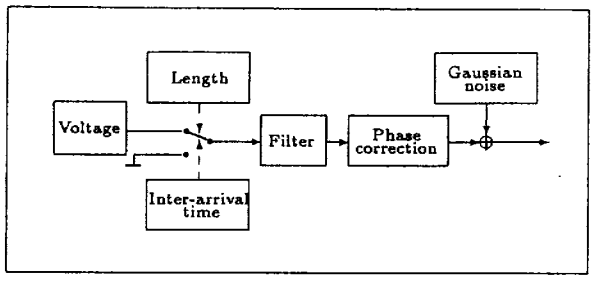

Fig. 12. Simulation block diagram.

Aside from the fact that the Dirac is reduced by the n-fold convolutions, it is quite difficult to prove that the shape of the density at the output of the filter $f_{\text{out}}(u)$ is nearly equal to the one of $f_i(u)$ after n convolutions. Only for small n, e.g., $n = 2, 3$, one still sees the dominance of the terms $f_1'(u)$ compared with convolution products thereof.

After all, the regeneration effect is due to the special shape of the density $f_i(x)$ and the special set of filter coefficients k_ν. Thus, the insertion of a Dirac into a density is not a generally applicable method.

Note that the coefficient 'u_0' will be different for the input and output densities. Hence, the corresponding coefficient at the input for a desired output density has to be determined in advance. Figure 11 shows an exemplary PDF at the output of the filter, which is obviously quite similar to the approximation by (2).

For other principal approaches to include spectral properties, see [17] and [18].

8.3 Simulation Scheme

After describing the different generators and the spectral properties in amplitude and phase, we are ready to present the whole simulation scheme in Fig. 12. It consists of generators for the voltage samples, the lengths and the inter-arrival times, where the activity of the first is controlled by the latter two. An FIR filter, whose impulse response is the IFFT of the square root of the mean PDS, ensures the spectral (amplitude) properties. An optional phase correction sets the phase according to (18). The phase correction consists of an FFT and thereafter, the phase is replaced by samples resulting from (18), whereas the amplitude is left unchanged. The filtering operation can, of course, be combined with the phase correction, which means a multiplication of the frequency response of the filter with the FFT spectrum of the voltage signal. After the phase correction an IFFT yields the desired impulsive noise.

The phase correction does not change the voltage statistics significantly. The effect on the length distribution has not yet been investigated.

Another possibility to simulate impulsive noise would be to read the impulses from a data bank (more than 10,000 impulses), which would be induced by random time samples from the inter-arrival time generator. The disadvantage is the necessity to store all the impulse events. All 51,200 impulses recorded at one location, e.g., demand for about 200 MBytes of memory even in compressed form.

The use of one representative impulse or a Markoff model is no alternative. The first lacks of the desirable statistical properties, while the second would be far too complex. Note that the probability of a certain gap length l_G (between impulses) would be described by

$$p_G(l_G = j) = \sum_{\nu=0}^{N_G-1} P_\nu \cdot (1 - q_\nu)^{j-1} q_\nu \qquad (29)$$

in the case of one burst (impulse) state and N_G gap states, where q_ν is the transition probability from gap state ν to the burst state and $(1 - q_\nu)$ is the probability to stay in gap state ν. P_ν is the probability to be in a special gap state ν under all gap states. (29) is a sum of functions that are of the type of the exponential density in (6). In order to approximate the real inter-arrival time distribution, too many states would be needed. This disqualifies the Markoff model for our application.

9. Conclusions

Results of a recent impulsive noise survey in the network of Deutsche Bundespost Telekom were presented. These led to analytic expressions for the most important statistical properties of this non-stationary disturbance. The voltage density can be approximated by a double exponential with a power to 1/5 in the exponent. Two alternatives for the inter-arrival time distribution have been discussed, one proposed earlier by Fano and a generalization of the Poisson law. The lengths of the impulses mostly followed a combination of two log-normal densities. Possible pseudo-noise generators for computer simulation were presented. A combination of all generators and a filter, representing the mean power-density spectrum, realizes all described properties. The simulation may be further improved by including the typical phase of impulsive noise. This may be done applying an FFT. Additionally, a 'representative' impulse has been derived that, unlike earlier proposals, looks like real measured impulses.

Acknowledgement

We would like to thank all of the people that helped performing the measurements, namely our colleagues Mr. Fahrendholz and Mr. Fydrich and all the persons responsible for the local switching offices. We greatly appreciate all their support.

A somewhat more comprehensive report (in German) can be obtained from the authors.

References

[1] Nadenau, J.: Typische Störspannungen in Fernsprechvermittlungsstellen. NTZ **15** (1962), 236–240.
[2] Berger, J. M.; Mandelbrot, B.: A new model for error clustering in telephone circuits. IBM J. Res. a. Develop. **7** (1963), 224–236.
[3] Fennick, J. H.: Amplitude distributions of telephone channel noise and a model for impulse noise. Bell Syst. Tech. J. **48** (1969), 3243–3263.
[4] Fano, R. M.: A theory of impulse noise in telephone networks. IEEE Trans. on Comm. COM-**25** (1977), 577–588.
[5] Wellhausen, H.; Fahrendholz, J.: Digitalsignalübertragung auf symmetrischen Ortsverbindungs- und Ortsanschlußkabeln. Tech. Rept. 442 TB 71, Darmstadt: FTZ, 1986.
[6] Messen des Störbelags auf OAsl für Frequenzen bis 200 kHz. Tech. Rept. (internal), Darmstadt: FTZ, 1987.
[7] Müller, W. F.; Lubenow, H.: Störimpulse in Nachrichtenkanälen. Nachr.tech., Elektronik **38** (1988), 8–9.
[8] Széchényi, K.; Böhm, K.: Impulsive noise limited transmission performance of ISDN subscriber loops. Proc. of ISSLS, 1988, 2.3.1–2.3.6.
[9] Széchényi, K.: On the NEXT and impulse noise properties of subscriber loops. Conf. Rec. GLOBECOM '89, Dallas, 1989, 1569–1573.
[10] Cook, J. W.: Wideband impulsive noise survey of the access network. BT Technol. J. **11** (1993), 155–162.
[11] Valenti, C. F.; Kerpez, K.: Analysis of wideband noise measurements and implications for signal processing in ADSL systems. ICC '94, Houston, TX, 1994.
[12] Oppenheim, A. V.; Schafer, R. W.: Digital signal processing. London: Prentice-Hall, 1975.
[13] Press, W. H.; Flannery, B. P.; Teukolsky, S. A.; Vetterling, W. T.: Numerical recipes, the art of scientific computing. Cambridge: Cambridge University Press, 1989.
[14] Knuth, D. E.: The art of computer programming, seminumerical algorithms. Vol. 2. 2nd ed. Massachusetts: Reading, 1981.
[15] Devroye, L.: Non-uniform random variate generation. Berlin: Springer, 1986.
[16] Walker, A. J.: An efficient method for generating random variables with general distributions. ACM Trans. on Math. Software **3** (1977), 253–256.
[17] Brehm, H.: Beschreibung und Erzeugung stochastischer Signalmodelle – insbesondere für telefonbandbegrenzte Sprache. Kleinheubacher Berichte, Darmstadt, 1989, 533–536.
[18] Johnson, G. E.: Constructions of particular random processes. Proc. of the IEEE **82** (1994), 270–285.

Werner Henkel was born in Gelnhausen, Germany, on April 27, 1960. He studied electrical engineering (telecommunications) at TH Darmstadt, where he received his diploma degree in 1984. From 1984 to 1989 he had a contract as a research assistant at TH Darmstadt and received his Ph.D. degree in 1989. His thesis was on coding with complex numbers. During this time, he also held lectures at FH Frankfurt. In 1989 he joined the Research Center of Deutsche Bundespost Telekom. His work concentrates on digital communications, especially coding, coded modulation, synchronization, equalizing, neural networks, and channel modeling. He also held internal courses on information theory and coding.

From September 1993 until March 1994 he was on a sabbatical leave at AT&T Bell Laboratories, Middletown, N.J., where he worked on high-rate subscriber line transmission in an impulsive noise environment and burst-error correcting codes.

Publications are on analog codes, coding and interpolation, Toeplitz algorithms, coded modulation, synchronization, channel modeling, burst error correcting codes, and A/D-conversion.

Thomas Keßler was born in Kassel, Germany, on February 22, 1961. He received his diploma degree in communications engineering from the Technical University of Braunschweig in 1987. Since then, he is with the Research Center of Deutsche Bundespost Telekom, department of digital transmission systems. He was engaged in the error-performance analysis of quaternary transmission systems, the digital signal processing for equalizers, and the design of rotationally invariant trellis codes. He was also involved in the hardware implementation of Viterbi decoders for both satellite and cable applications. His current interest is in the analysis of measured impulsive noise on telephone cables and its modeling for computer simulations.